



Mechanism of CO₂ hydrogenation over Cu/ZrO₂($\bar{2}12$) interface from first-principles kinetics Monte Carlo simulations

Qi-Jun Hong, Zhi-Pan Liu *

Shanghai Key Laboratory of Molecular Catalysis and Innovative Materials, Department of Chemistry, Key Laboratory for Computational Physical Science (Ministry of Education), Fudan University, Shanghai 200433, China

ARTICLE INFO

Article history:

Received 5 April 2010

Accepted 16 July 2010

Available online 27 July 2010

Keywords:

Heterogeneous catalysis

Density functional calculations

Kinetic Monte Carlo

Metal/oxide

CO₂ fixation

Cu/ZrO₂

ABSTRACT

It has been a goal consistently pursued by chemists to understand and control the catalytic process over composite materials. In order to provide deeper insight on complex interfacial catalysis at the experimental conditions, we performed an extensive analysis on CO₂ hydrogenation over a Cu/ZrO₂ model catalyst by employing density functional theory (DFT) calculations and kinetic Monte Carlo (kMC) simulations based on the continuous stirred tank model. The free energy profiles are determined for the reaction at the oxygen-rich Cu/m-ZrO₂($\bar{2}12$) interface, where all interfacial Zr are six-coordinated since the interface accumulates oxidative species at the reaction conditions. We show that not only methanol but also CO are produced through the formate pathway dominantly, whilst the reverse-water-gas-shift (RWGS) channel has only a minor contribution. H₂CO is a key intermediate species in the reaction pathway, the hydrogenation of which dictates the high temperature of CO₂ hydrogenation. The kinetics simulation shows that the CO₂ conversion is 1.20%, the selectivity towards methanol is 68% at 500 K and the activation energies for methanol and CO formation are 0.79 and 1.79 eV, respectively. The secondary reactions due to the product readsorption lower the overall turnover frequency (TOF) but increase the selectivity towards methanol by 16%. We also show that kMC is a more reliable tool for simulating heterogeneous catalytic processes compared to the microkinetics approach.

© 2010 Elsevier B.V. All rights reserved.

1. Introduction

The chemical conversion of CO₂ is of great interest nowadays because it not only removes this greenhouse gas but also yields useful fuels and chemicals such as methanol. As shown in formula (1), methanol can be produced by the hydrogenation of CO₂. Metal and metal oxide composites are the typical catalysts for the hydrogenation of CO₂. However, it is common in practice that the hydrogenation also produces CO, which is believed to be formed through the RWGS in formula (2).



$$\Delta H_{500\text{K}} = -62.62 \text{ kJ/mol [1]}, \Delta G_{500\text{K}} = 37.81 \text{ kJ/mol}$$



$$\Delta H_{500\text{K}} = 39.88 \text{ kJ/mol}, \Delta G_{500\text{K}} = 20.21 \text{ kJ/mol}$$

The formation of methanol is an exothermal reaction and its selectivity drops with the increase of temperature. Therefore catalysts operating at relatively low temperatures are thermodynamically

desirable. Campbell and coworkers have demonstrated that pure Cu can act as a catalyst for methanol synthesis [2,3]. Aiming to find the best catalyst with both high activity and high selectivity, a variety of oxide-supported Cu catalysts has been tested. While Cu/ZnO systems are most often used in practice, ZrO₂-supported Cu (Cu/ZrO₂) catalyst with good thermal stability, high activity and selectivity has attracted much attention [4,5].

To date, a large volume of experimental work [5–11] has been reported on the catalytic performance of Cu/ZrO₂ catalyst. Bell and coworkers [12,13] have shown that there is a significant enhancement in both activity and methanol selectivity if ZrO₂ is added into Cu/SiO₂ catalyst. It was suggested that ZrO₂ helps in the adsorption of CO₂, while Cu is a reservoir of surface hydrogen. Therefore the Cu/ZrO₂ interface was proposed to be the reaction site [14]. For the reaction mechanism, two most popularly suggested routes are the formate pathway and the RWGS pathway. Using in situ diffuse reflectance FTIR spectroscopy, Fisher and Bell [13] have identified a large amount of formate on the surface. They suggested that the reaction proceed via the hydrogenation of CO₂. However, it remains uncertain whether formate is an active intermediate or merely a spectator of the reaction. Using the same technique, Weigel et al. [15,16] found adsorbed formaldehyde and proposed a pathway involving the dissociation of CO₂ to CO. The subsequent hydrogenation of CO can finally produce methanol. They also showed that the surface concentration of formate

* Corresponding author. Tel./fax: +86 21 6564 2400.

E-mail address: zpliu@fudan.edu.cn (Z.-P. Liu).

is rather constant with the production of methanol. Based on this fact, they excluded the formate pathway as the main reaction channel. Using DFT and microkinetics, the water-gas shift (WGS) reaction on pure Cu has been investigated recently [17].

In our previous theoretical study [18], we have utilized the first principles DFT method to identify the mechanism for methanol synthesis at the Cu/ZrO₂ interface. We showed that the interface can indeed work as the catalytic center and both formate pathway and RWGS pathway are likely. In this work, we provide a complete, self-consistent kinetics description on the whole process and aim to fully resolve the mechanism at the experimental conditions. We establish the free energy profile with all DFT energetics corrected with ZPE and entropy. By performing dynamic kMC simulation, we determine the rate, selectivity and activation energies of the reaction. The secondary reaction processes due to the readsorption of products are considered and found to contribute significantly to both the rate and the selectivity. Our theoretical results show that the formate pathway initiated by the direct hydrogenation of CO₂ is the dominant pathway at the oxygen-rich Cu/ZrO₂ interface, although the formate concentration at the interface is quite constant.

2. Theoretical methodology and models

All DFT periodic slab calculations were performed using SIESTA code [19,20]. The exchange-correlation functional utilized was at the level of Perdew–Burke–Ernzerf (PBE) generalized gradient approximation [21]. For all elements, the basis set was expanded with the double- ζ plus polarization numerical atomic orbitals and Troullier–Martins norm-conserving pseudopotential [22] was used to treat the core electrons. For Zr, the semi-core states (4s, 4p) were included as valence states [23]. A radii confinement of the orbitals was set as equivalent to an energy shift of 0.01 eV. The kinetic energy cutoff for the real-space mesh used to represent the density was specified to be 150 Ry. As the chosen supercells were rather large, only the Γ -point was employed for the first Brillouin zone integration. Geometry optimization was performed by the Quasi-Newton–Broyden method until all the remaining forces acting on each relaxed atom were below 0.05 eV/Å. Transition states of all the catalytic reactions are searched with our recently-developed Constrained–Broyden–Minimization method [24] and the Broyden-dimer method [25,26]. Convergence of reported reaction energies and barriers was verified (within 0.1 eV) with regard to the basis set, energy shift and kinetic energy cutoff and k -point sampling grid. For example, for CO₂ adsorption at the interface, the calculated adsorption energy is 0.69 and 0.70 eV with the Γ -point and the ($4 \times 4 \times 1$) k -point samplings, respectively.

Monoclinic ZrO₂ was chosen as our model for the support because ZrO₂ is one of the best oxide supports and Cu/m-ZrO₂ was reported to have much higher activity and selectivity for methanol synthesis from CO₂/H₂ than Cu supported on tetragonal ZrO₂ [27]. Theoretically, the surface structure and stability of ZrO₂ were thoroughly investigated by Christensen and Carter [28] using the plane-wave DFT method. The current DFT functional can predict correctly the large band gap property [28] and the irreducibility (high activation in O-vacancy generation) [18] of ZrO₂ surfaces. They showed that the flat ($\bar{1}11$) facet is the most stable surface of m-ZrO₂ and the stepped ($\bar{2}12$) facet depicts the most common stepped sites. In our modeling, the two surfaces of monoclinic ZrO₂ were simulated by 3-layer slabs with a vacuum spacing of 16 Å. Large unit cells were employed: $p(2 \times 2)$ [13.629×14.746 Å and 48 formula units of ZrO₂] for the ($\bar{1}11$) facet; $p(3 \times 1)$ [20.443×11.693 Å and 54 formula units of ZrO₂] for the ($\bar{2}12$) facet. The topmost 16 ZrO₂ units and 24 ZrO₂ units were allowed to be relaxed for the two surfaces. Slab thickness was checked in order to achieve convergence. The difference of CO₂ adsorption energy calculated in the 3-layer and 4-layer slabs is at most 0.02 eV. To validate our DFT calculation setups, the chemical adsorption of CO₂ on bare m-ZrO₂ ($\bar{1}11$) (flat surface) and ($\bar{2}12$) (stepped surface) was first

studied. The calculated CO₂ adsorption energies are 0.83 and 1.58 eV for the two surfaces, which are in accordance with those measured by experiment (0.75–1.51 eV) [29].

As already utilized in our previous work [18], the optimized Cu/ZrO₂ model is shown in Fig. 1, where the Cu is charge neutral with the composition being Cu₃₂Zr₅₄O₁₀₈ per slab. It should be mentioned that a large $p(3 \times 1)$ unit cell was utilized to allow for a better lattice match between Cu and ZrO₂ (mismatch $\approx 0.4\%$, referred to the direction along the Cu strip, i.e. eight Cu–Cu lattice distances with respect to six Zr–Zr distances in bulk ZrO₂ lattice). The structure of the Cu/ZrO₂ system was firstly relaxed by first principles molecular dynamics with Nose thermostat at 200 K for ~ 1 ps; the energetically favorable structures from the MD trajectories were then selected and optimized by the Broyden method. We found that this strategy is essential in order to prevent the composite structure trapping into a local minimum on the potential energy surface. In the optimized structure, only the most stable facets of the two components, namely the ($\bar{1}11$) terrace of ZrO₂ and (111)-like Cu surface, are exposed. Both O and Zr atoms from ZrO₂ interact with the Cu strip. Two kinds of Zr, the five-coordinated (Zr_{5c}) and six-coordinated (Zr_{6c}) lattice Zr are exposed, which are separated by oxygen atoms at the interface. Thus the interface between the oxide step-edge and the Cu strip can be viewed as an array of periodic Zr_{5c}–O–Zr_{6c}–O linkages, namely, a mixed Zr_{5c}/Zr_{6c} model for the interface. Our previous work has shown that a significant portion of the interfacial Zr sites, mainly Zr_{5c}, were found to be terminated by extra oxidative species [18], leading to the partially oxidized interfacial Cu. This is mainly due to the fact that exposed Zr_{5c} sites at the interface bind too strongly with the oxidative species and once they are available, they will quickly be capped by oxidative intermediates in reaction. In this work, we therefore adopt the oxygen-rich interface as our model to mimic the real catalyst under experimental conditions, where the exposed Zr_{5c} sites are already blocked by the oxygen species. Based on this principle, we computed all DFT energetics for the adsorbates preferentially on six-coordinated Zr (Zr_{6c}). These data can then be utilized to represent the situation in the oxygen-rich interface, simply because once a Zr_{5c} site is occupied by an additional oxidative species, the Zr_{5c} turns into a Zr_{6c} site. By switching to the Zr_{6c} model, we have to recalculate all the elementary reactions and determine the new reaction profile. We found that the adsorption energies of oxygen-containing species like O and H₃CO are indeed much reduced at the Zr_{6c} model, which effectively prevents the poisoning of the model catalyst in the kinetics simulation. The validity of the Zr_{6c} model is then checked by kMC simulation and the results are extensively compared with experiment.

The kMC technique [30] enables us to deal with complex systems on time scales of the order of seconds or even longer, which cannot be achieved by typical molecular dynamics simulations. First principles kMC simulations have been performed on a variety of systems [31–35] in recent years. It has been shown that this technique can deal with complex reaction system with good accuracy when compared with experiments. The Bortz–Kalos–Lebowitz algorithm [36] was utilized in our kMC simulation. The detail of the simulation setup has been addressed in our previous paper [18]. In order to obtain the free energy profile for the kinetics simulation, we have performed vibrational frequency analysis to calculate ZPE and entropy of all the states involved in the reaction. The free energy barriers ΔG^\ddagger of the elementary reactions are calculated as follows:

$$\Delta G^\ddagger = \Delta E_{OK}^\ddagger + \Delta(\Delta E_{OK \rightarrow T}^\ddagger) + \Delta ZPE^\ddagger - T\Delta S^\ddagger$$

$$\Delta ZPE^\ddagger = \frac{1}{2}h(\sum \nu_{\text{transition state}} - \sum \nu_{\text{initial state}})$$

$$\Delta S^\ddagger = k \ln \left(\frac{q_{\text{transition state}}}{q_{\text{initial state}}} \right)$$

where ν is the vibration frequency and q is the partition function.

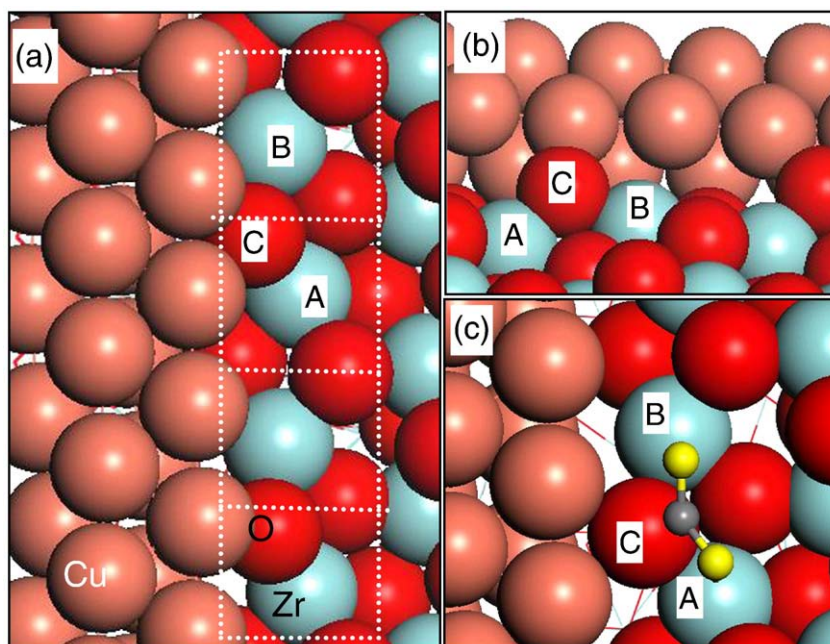


Fig. 1. (a) Top and (b) side view of optimized structure of Cu strip at the stepped $m\text{-ZrO}_2(\bar{2}12)$, and (c) the structure of CO_2 adsorption. The white dotted lines in (a) represents schematically the 1-D grid utilized in kMC simulation, each containing a Zr site at the interface. A, Zr_{6c} ; B, Zr_{5c} ; C, O_{2c} . Lattice O, red; Cu, orange; Zr, cyan; C, grey; O of CO_2 , yellow.

For reaction (1) and (2), the reaction energies directly from thermodynamic data should be in principle the same as those we computed from DFT by summing up all the elementary steps. Unfortunately, the current DFT methods are known to be inaccurate for calculating the reaction energy. The enthalpy changes of reactions (1) and (2) are calculated to be -0.85 and 0.80 eV, respectively, while the experimental counterparts are -0.65 and 0.41 eV. Although qualitative agreement is achieved by DFT, the absolute errors are quantitatively large and will lead to unrealistic results in kinetics. We also noticed that the error cannot be significantly reduced by augmenting the basis (such as utilizing the plane wave methodology) or switching the exchange-correlation functional to the standard B3LYP. In order to solve this problem, it is necessary in practice to adjust the DFT values to match the experimental enthalpy. In this work, we confined our adjustment of DFT values to the adsorption energies of molecules, and kept the data of the surface reactions untouched since DFT-PBE has been demonstrated to be reasonably accurate for surface reactions. To match the experimental enthalpy change, the adjustment of the adsorption energies must satisfy the following two equations.

$$\begin{cases} \Delta E_{\text{H}_3\text{COH}} + \Delta E_{\text{H}_2\text{O}} - \Delta E_{\text{H}_2} \times 3 - \Delta E_{\text{CO}_2} = -0.65 - (-0.85) \\ \Delta E_{\text{CO}} + \Delta E_{\text{H}_2\text{O}} - \Delta E_{\text{H}_2} - \Delta E_{\text{CO}_2} = 0.41 - 0.80 \end{cases}$$

In this work we set $\Delta E_{\text{CO}_2} = 0$, $\Delta E_{\text{H}_2} = -0.242$, $\Delta E_{\text{H}_3\text{COH}} = -0.2$, $\Delta E_{\text{CO}} = -0.5$, $\Delta E_{\text{H}_2\text{O}} = -0.141$ eV according to three guidelines as follows. First, the adjustment should be as small as possible. We did not modify CO_2 adsorption energy as it is close to the values determined from experiments. Second, the DFT-PBE adsorption energies of CO on Cu were known to be inaccurate by several tenths eV (0.3 – 0.5 eV) [37]. Third, the adjustment should be negative (i.e. reducing adsorption energy), if not zero, because DFT-PBE tends to overestimate the adsorption energy in general.

3. Results

3.1. DFT calculation of the reaction pathways

CO_2 adsorbs preferentially on ZrO_2 sites of the Cu/ZrO_2 surface. The calculated adsorption energies (E_{ad}) of CO_2 on terrace ZrO_2 , at the

interface and on Cu are 0.83 , 0.69 and 0.06 eV respectively, confirming that ZrO_2 serves as the adsorption sites for CO_2 [14]. On the other hand, the dissociative adsorption of H_2 only occurs on Cu. The E_{ad} of H atom at Cu hcp site is 0.52 eV with respect to the gas phase H_2 molecule, while H_2 can hardly dissociate on ZrO_2 . These results are in accordance with the earlier finding that Cu acts as a reservoir of hydrogen in the reaction [14]. With the Zr_{6c} interface model, we have obtained all the kinetics data for the two reaction routes (the RWGS route and the formate route), which are summarized in Table 1. The two reaction routes are further elaborated as follows.

3.1.1. RWGS route

In this route, the adsorbed CO_2 dissociates directly at the interface, forming the adsorbed CO and atomic O. By stepwise hydrogenation to formyl (HCO) and formaldehyde (H_2CO), CO is converted to methanolate (H_3CO). H_3CO is one of the most abundant species observed in experiments [13,15]. H_3CO can further be hydrogenated to methanol (H_3COH). Meanwhile, the surface atomic O can react with H to form hydroxyl and water.

3.1.2. Formate route

In parallel with the RWGS pathway, the adsorbed CO_2 can alternatively react with H to yield the surface formate (HCOO). This species was commonly detected in experiments [13,15]. Upon further hydrogenation, HCOO is converted to H_2COO and H_2COOH . These species, including HCOO , H_2COO and H_2COOH , adsorb bidentately at the interface. The interfacial H_2COOH can dissociate to formaldehyde (H_2CO) and hydroxyl (OH), which may further be hydrogenated to methanol and water, respectively. The free energy profile of this path is shown in Fig. 2. The HCOO and H_2COO are the most stable intermediates, while H_2COOH and H_2CO are the least stable surface species. We also checked other possible channels for the hydrogenation of formate, such as the one involving HCOOH . But they are excluded from our proposed mechanism because these species and the pathways related are not favored both kinetically and thermodynamically.

Table 1

Kinetic parameters (eV) from DFT for the elementary steps involved in methanol synthesis at the interface of Cu/ZrO₂ (*T* = 500 K).

Elementary step		$\Delta E^{\ddagger a}$	$\Delta ZPE^{\ddagger c}$	$-\Delta S^{\ddagger c}$	$\Delta G^{\ddagger c}$
CO ₂ + 2* ⇌ CO ₂ ** ^b	Forward	0	0	1.06	1.06
	Reverse	0.75	-0.10	0	0.66
CO ₂ ** ⇌ CO* + O*	Forward	0.91	-0.11	0.00	0.80
	Reverse	0.85	0.03	0.13	1.00
CO* + H# ⇌ HCO*	Forward	1.01	-0.04	0.00	0.97
	Reverse	1.11	-0.17	-0.08	0.86
HCO* + H# ⇌ H ₂ CO*	Forward	0.39	0.00	0.03	0.43
	Reverse	0.52	-0.13	0.06	0.45
H ₂ CO* + H# ⇌ H ₃ CO*	Forward	1.07	-0.03	-0.01	1.03
	Reverse	1.53	-0.18	0.09	1.44
H ₃ CO* + H# ⇌ H ₃ COH*	Forward	1.28	-0.06	0.04	1.25
	Reverse	0.68	-0.22	-0.03	0.42
O* + H# ⇌ OH*	Forward	0.88	-0.08	-0.02	0.79
	Reverse	0.88	-0.17	0.04	0.75
OH* + H# ⇌ H ₂ O*	Forward	0.93	-0.04	0.00	0.89
	Reverse	0.54	-0.18	0.03	0.39
CO ₂ ** + H# ⇌ HCOO**	Forward	0.54	-0.02	0.03	0.55
	Reverse	1.30	-0.10	0.15	1.35
HCOO** + H# ⇌ H ₂ COO**	Forward	0.68	-0.05	0.06	0.69
	Reverse	0.83	-0.20	-0.04	0.59
H ₂ COO** + H# ⇌ H ₂ COOH**	Forward	1.30	-0.06	0.01	1.26
	Reverse	0.54	-0.19	0.01	0.37
H ₂ COOH** ⇌ H ₂ CO* + OH*	Forward	0.65	-0.16	-0.09	0.40
	Reverse	0.68	0	0	0.68
CO* ⇌ CO + *	Forward	1.09	-0.05	0	1.04
	Reverse	0	0	0.85	0.85
H ₃ COH* ⇌ H ₃ COH + *	Forward	0.95	-0.05	0	0.90
	Reverse	0	0	1.12	1.12
H ₂ O* ⇌ H ₂ O + *	Forward	0.82	-0.07	0	0.74
	Reverse	0	0	0.86	0.86

^a The energy difference between the transition state and the initial or the final state (reaction barrier).

^b * and ** represent the monodentate and the bidentate species, respectively.

^c # represents the adsorption site on Cu.

3.2. kMC simulations

3.2.1. General setup of kMC simulation

With the free energy profile of the catalytic system calculated, we were able to utilize the kMC technique to simulate the whole reaction process. In addition to the elementary steps listed in Table 1, we also took into account fast reaction steps, including the diffusion of CO,

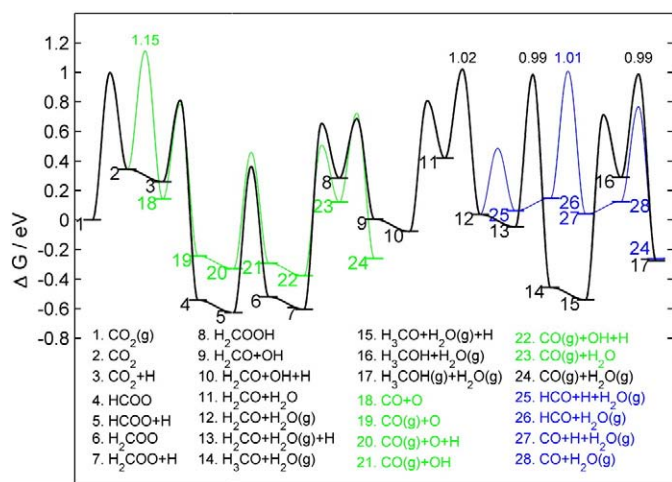


Fig. 2. Free energy profile of the calculated reaction pathways in methanol synthesis from CO₂ hydrogenation (*T* = 500 K). For simplicity, H₂ in the gas phase (H₂(g)) that is required for mass balance is omitted in the text (in total six H are needed per CO₂ conversion).

H₂O and H₃COH species, and the proton transfer among H₃CO, H₃COH, O, OH and H₂O. These fast reaction steps are of importance to the overall reaction rate. Diffusion may help to increase the overall reaction rate because it can free more surface sites for CO₂ adsorption (we will discuss this in depth in Section 4.1). Proton transfer may contribute to the formation of surface water and methanol, which in turn accelerates the desorption of products.

In order to facilitate the kMC simulation, we have simplified our kinetics model in two aspects, which have already been utilized previously [18]. First, since both our DFT calculation and experimental results indicate that the reaction occurs at the interface, we limit our kMC lattice model to one dimension. This simplification is reasonable because the intermediates are generally more stable at the interface region than on the sites of either Cu or ZrO₂. Second, the adsorption and desorption of hydrogen on Cu are treated as quasi-equilibrium. This approximation is based on the fact that the diffusion of hydrogen on Cu is several orders of magnitude faster than the hydrogenation and dehydrogenation (the diffusion barrier of H atom on Cu is only about 0.1 eV). Moreover, in order to verify that our simplifications and approximations are indeed reasonable and do not lead to biased results, we first performed a kMC simulation in a closed system until the equilibrium is established.

3.2.2. Equilibrium simulation

According to the experimental results, the free energy changes of reaction (1) and (2) at 500 K are 0.393 and 0.210 eV, respectively [1]. With the total pressure 17 atm and the molar ratio of CO₂ to H₂ 1:3, the theoretical conversion of methanol and CO can be derived as follows. At the equilibrium, the pressures (in atm) of H₃COH and CO are denoted as $p_{\text{H}_3\text{COH}}$ and p_{CO} , respectively. The pressures of water, CO₂ and H₂ are thus $p_{\text{H}_3\text{COH}} + p_{\text{CO}}$, $\frac{17.0}{4} - p_{\text{H}_3\text{COH}} - p_{\text{CO}}$ and $\frac{17.0}{4} \times 3 - 3 \times p_{\text{H}_3\text{COH}} - p_{\text{CO}}$, respectively. The thermodynamics equilibrium of the reactions can be described by the following equations.

$$\left\{ \begin{array}{l} \frac{p_{\text{H}_3\text{COH}} \cdot (p_{\text{H}_3\text{COH}} + p_{\text{CO}})}{\left(\frac{17.0}{4} - p_{\text{H}_3\text{COH}} - p_{\text{CO}}\right) \cdot \left(\frac{17.0}{4} \times 3 - 3 \times p_{\text{H}_3\text{COH}} - p_{\text{CO}}\right)} = e^{-\frac{0.393 \times 1.6 \times 10^{-19}}{1.38 \times 10^{-23} \times 500}} \\ \frac{p_{\text{CO}} \cdot (p_{\text{H}_3\text{COH}} + p_{\text{CO}})}{\left(\frac{17.0}{4} - p_{\text{H}_3\text{COH}} - p_{\text{CO}}\right) \cdot \left(\frac{17.0}{4} \times 3 - 3 \times p_{\text{H}_3\text{COH}} - p_{\text{CO}}\right)} = e^{-\frac{0.210 \times 1.6 \times 10^{-19}}{1.38 \times 10^{-23} \times 500}} \end{array} \right.$$

By solving these equations, we get $p_{\text{H}_3\text{COH}} = 0.542$ atm, $p_{\text{CO}} = 0.324$ atm. Therefore according to thermodynamic data, the conversion to methanol and CO is:

$$C_{\text{H}_3\text{COH}} = \frac{p_{\text{H}_3\text{COH}}}{p_{\text{CO}_2 \text{ init}}} = \frac{0.542}{17.0/4} = 12.8\%$$

$$C_{\text{CO}} = \frac{p_{\text{CO}}}{p_{\text{CO}_2 \text{ init}}} = \frac{0.324}{17.0/4} = 7.6\%$$

To compare theoretical results with the above values from experimental data, the kMC simulation in a closed system was performed. This is a good way to verify the energetics utilized in the kMC simulation. Our kMC model contains 1000 reactive sites (lattice model), 100,000 CO₂ and 300,000 H₂ molecules. The temperature and pressure are 500 K and 17 atm, respectively. The simulation is stopped until all the data are statistically steady and the detailed balance condition is reached. At the equilibrium, we found that there are statistically 80,633 CO₂, 6154.5 CO and 12,393 H₃COH on average in the gas phase. The conversion ratios to methanol and CO are thus determined to be 12.5% and 6.2% respectively, which are consistent with the above-derived values (12.8% and 7.6%). Therefore, it indicates that the reaction profile utilized in kMC model is valid and, importantly, the approximations we made do not lead to significant deviation thermodynamically.

3.2.3. Dynamic simulation

Different from the closed system, the typical catalytic experiments operate under a dynamic environment where the input gas continuously flows through the reactor. To simulate this, we designed our model based on the continuous stirred tank reactor model. Compared to the simulation of the closed system, there are two extra parameters in the dynamic model: the ratio of reactant flow to catalytic sites (for example, the number of CO₂ molecules added into the reactor per second per site) and the contact time. The former represents the ratio of reactants to catalysts. The higher the ratio, the lower the conversion is. The latter is related to the effective time for the reaction. If reactants are allowed to stay in the reactor for a longer period, they would be more likely to be converted to products.

According to the typical experimental setup [38], we set temperature and pressure to 500 K and 17 atm. The gas flow is 90 cm³ min⁻¹ (H₂/CO₂ = 3, STP) and the weight of catalyst is 1 g with the Cu surface area 6.3 m²/g. Therefore, the ratio of CO₂ flow to catalytic sites is approximately 0.1.

$$\frac{N_{\text{CO}_2}}{N_{\text{site}}} = \frac{\frac{r}{1+\beta} \times \frac{P}{RT} \times N_A}{m \times S \times \gamma} = \frac{90 \div 60 \div 4 \div 22400 \times 6.02 \times 10^{23}}{1 \times 6.3 \times 1.46 \times 10^{19}} = 0.1$$

(where r is the rate of the flow; P is pressure; R is ideal gas constant; T is temperature; m is mass of the catalyst; S is the ratio of surface area to mass; and γ is the number of sites per unit surface area.)

As for the contact time, it is often not mentioned explicitly in experimental literatures. Here we set the volume of the reactor as 1.75 cm³ [15]. The contact time is calculated to be 10 s, which means that 10% of the molecules in the gas phase flow out the reactor every second.

$$t = \frac{n_r}{n_f} = \frac{P_r V_r / T_r}{P_f r / T_f} = \frac{1.75 \times 17 / 500}{90 / 60 / 273} = 10 \text{ s}$$

(where P_r is pressure of the reactor; V_r is volume of the reactor; T_r is temperature of the reactor; P_f is pressure of the gas flow; r is gas flow rate; T_f is temperature of the gas flow.)

The detail of our dynamic kMC model is described as follows. There are 10,000 catalytic sites and all the sites are empty initially, together with 10,000 CO₂ and 30,000 H₂ in the system. Once the simulation starts, 1000 CO₂ and 3000 H₂ molecules are added into the chamber per second, and meanwhile 10% of the gases in the system are removed per second as outflow. In real simulation, the time step of inflow and outflow is much less than 1 second. We added 0.1 CO₂ and 0.3 H₂ into the system and removed 0.001% of the gases every 0.0001 second in order to reduce fluctuation in the composition of system. The addition or removal of molecules is treated at the fixed input or output rate.

Our dynamic model is sufficient for us to capture the nature of the continuous stirred tank reactor. Except for the inflow and outflow, there are no other ways to change the mass of system. Therefore it obeys the law of the conservation of matter and the classic mole

Table 2

Conversion, selectivity and TOF at different temperatures from kMC.

T (K)	Number of molecules			Conversion ^a	Selectivity ^b	TOF/s ⁻¹ × 10 ^{3c}
	CO ₂	H ₃ COH	CO			
500	9.88 × 10 ³	80.8	39.0	1.20%	67.4%	2.40
510	9.77 × 10 ³	133	97.4	2.30%	57.7%	4.60
520	9.57 × 10 ³	200	230	4.30%	46.5%	8.60
530	9.27 × 10 ³	263	469	7.32%	35.9%	14.6
540	8.87 × 10 ³	305	822	11.3%	27.1%	22.6

^a Conversion is calculated as $(n_{\text{H}_3\text{COH}} + n_{\text{CO}})/(n_{\text{CO}_2} + n_{\text{H}_3\text{COH}} + n_{\text{CO}})$.

^b Selectivity is calculated as $n_{\text{H}_3\text{COH}}/(n_{\text{H}_3\text{COH}} + n_{\text{CO}})$.

^c TOF is calculated as $(n_{\text{H}_3\text{COH}} + n_{\text{CO}})/10/10,000 \times 2$ (Since it involves always two reactive sites in a catalytic cycle, we define TOF per pair of catalytic sites.).

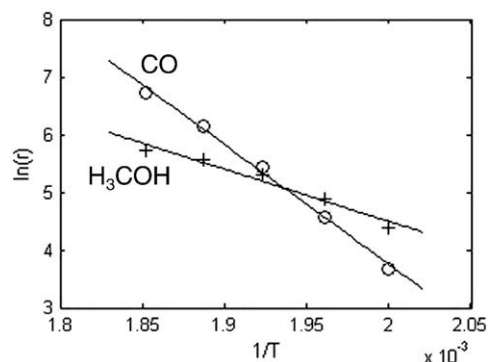


Fig. 3. Arrhenius plot to determine the apparent activation energy of H₃COH and CO formation. Circle: CO; Plus: H₃COH.

balance equations. (For example, one can find that the conservation of carbon atoms is obeyed from the results listed in Table 2.)

The major results from the kMC simulation of the continuous stirred tank model are listed in Table 2. As shown, the conversion of CO is found to be 1.20%, with the selectivity to methanol being 68%. The calculated turnover frequency (TOF) is $2.4 \times 10^{-3} \text{ s}^{-1}$, which falls in the range of experimental measurements [35] (see Table 2). Interestingly, we also noticed that methanol is dominantly produced from the formate channel, which will be further discussed later.

To further obtain the apparent activation energy, we performed kMC simulations from 500 to 540 K, with a step of 10 K to calculate the activation energy of methanol synthesis and CO formation. As shown in Fig. 3, the calculated activation energy of methanol and CO is 0.79 and 1.79 eV, respectively. According to the Arrhenius equation, the higher the activation energy is, the greater the impact of temperature will be on the reaction rate. Therefore the rate of CO increases much more rapidly than that of H₃COH as the temperature increases. This is the reason why the selectivity to methanol declines rapidly as temperature increases [12].

With the kMC simulation, it is possible for us to compare the key surface species from our results with those observed in experiment, for example, the in situ IR spectrograph by Bell and Baiker groups (Fig. 8 in Ref. 12). Fig. 4 plots the evolution of the coverage of the key species during the reaction. We found that formate, H₂COO and CO are produced almost instantaneously as the reaction starts. This is indeed in consistent with the experimental observation. Although the coverage of formate decreases slightly in the first 10 min (from 56% to 42%), the coverage of these three species is relatively constant in the reaction period. On the contrary, no H₃CO is formed at the beginning of the reaction and its concentration increases continuously in the next few minutes, which is also consistent with the observation in the experiment.

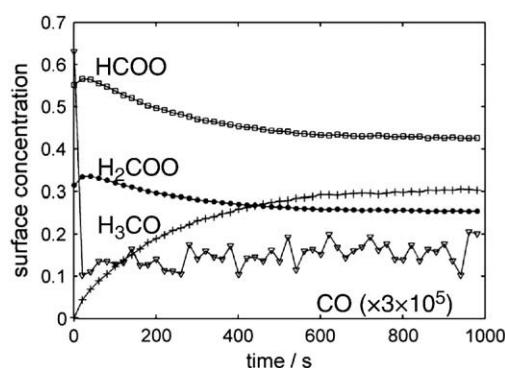


Fig. 4. The variation of surface coverage of reaction intermediates during the reaction. Square: HCOO; Circle: H₂COO; Plus: H₃CO; Triangle: CO.

Since the kMC results agree generally with the experimental findings in both the important kinetics quantities (e.g. activation energy, TOF) and the profile of reaction intermediates, we are at the better position to address which pathway contributes more to the formation of methanol at the experimental conditions. During our kMC simulation, we have counted the occurrence times of the forward (n_{forward}) and reverse (n_{reverse}) reactions of every elementary step. For a particular elementary step, we can identify easily the direction of this elementary step by calculating $n_{\text{forward}} - n_{\text{reverse}}$. In Table 3, we listed these numbers of some key reaction steps. From Table 3, we can see that the formate pathway is in fact the major reaction channel for CO_2 hydrogenation at the Cu/ZrO₂ interface since CO_2 decomposition rarely occurs. The entire simulation process can be described statistically as follows.

Over the 1518-second simulation period, 22,832 CO_2 molecules adsorb onto the catalytic surface and turn into other species. Most of them (96.6% = 22,045/22,832) experience the formate intermediate and then dissociate to formaldehyde. Formaldehyde can either react with surface hydrogen to methanol or dehydrogenate to CO. Among 5638 CO molecules produced, a large proportion of them (86.0% = 4851/5638) are originated from H_2CO , which are from the dissociation of H_2COOH via the formate pathway. This result is interesting because CO is most often considered as a product from the RWGS pathway. However, our results show that not only methanol but also CO are produced mainly via the formate route because the CO_2 direct dissociation at the interface is slow.

Finally, we can summarize the overall mechanism in the flow chart shown in Fig. 5, where the contribution of each channel in percentage is quantified with reference to a normalized 100% CO_2 input. Clearly, the reaction proceeds dominantly (96%) via the formate route: even the byproduct CO is generated mainly via the decomposition of HCO, instead of the direct dissociation of CO_2 . Because the dissociation of CO_2 is the slowest step in the entire process, it is largely circumvented and the formate pathway becomes dominant. As indicated by the occurrence times in Table 3, the other three elementary steps, namely, the adsorption of CO_2 , the hydrogenation of H_2CO (leading to methanol) and the dehydrogenation of HCO (leading to byproduct CO), are among the slowest steps and thus are the rate-controlling steps in the CO_2 hydrogenation process. It is interesting to notice that there are multiple reactions with comparable low rate in CO_2 hydrogenation. While the adsorption of CO_2 can be facilitated by lowering the temperature, the hydrogenation of H_2CO is a surface reaction, which places the low limit for the working temperature of CO_2 hydrogenation. Since the low temperature is desirable for methanol production due to thermodynamics, it is essential in the

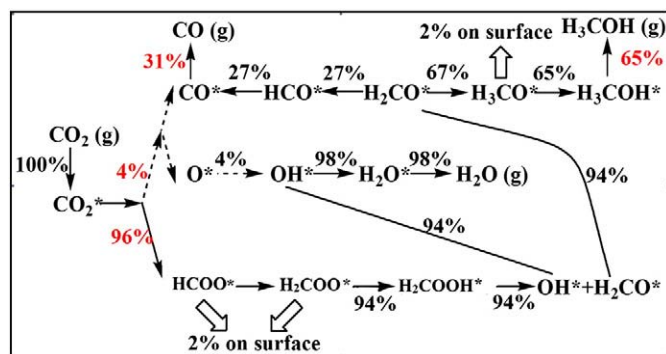


Fig. 5. Proposed reaction mechanism according to our kMC simulation results. Solid and broken lines are the major and minor routes, respectively. The percentage labeled on the arrows show contributions of elementary steps.

future work to focus on the stability of H_2CO species and the hydrogenation barrier of H_2CO for the design of new CO_2 utilization catalysts.

4. Discussion

4.1. Comparison between kMC and microkinetics methods

The microkinetics method is a mean-field approach and has been most commonly used in chemistry to deal with reaction kinetics. However, there have been objections in its application in some heterogeneous catalytic systems [39–43] due to the presence of fluctuations, lateral interactions, surface heterogeneity and limited mobility of adsorbates. For example, recently Temel et al. showed that microkinetics simulation with the correct rate constants fails to reproduce the kinetic behavior from kMC for CO oxidation on RuO₂ model catalyst, where the kMC results agree well with the experimental data [43]. Generally speaking, microkinetics is insufficient to account for fluctuations [42,43] and has difficulty in explaining some of the unusual observations when the system is highly history dependent and periodic [44]. It is therefore of interest to further compare the simulation results from microkinetics with those from kMC based on the same set of kinetics parameters. We find that although the simulation results are almost the same at the equilibrium, they differ significantly in dynamics.

Using microkinetics, we obtained that the calculated conversion of CO_2 to H_3COH and CO are 3.41% and 1.93%, respectively at 500 K and 17 atm. The turnover frequency is $1.1 \times 10^{-2} \text{ s}^{-1}$. All these values are about 5 times larger than what we obtained from kMC. In addition, the concentrations of surface species are very different from those in kMC, as shown in Fig. 6. The discrepancies between these two methods may be understood as follows. Taking CO_2 adsorption as an example, CO_2 is a

Table 3

The occurrence times (N_{occur}) of key reaction steps over a 1518-second simulation period from kMC.

Reaction		N_{occur}	ΔN_{occur}
$\text{CO}_2 + 2^* \rightleftharpoons \text{CO}_2^{**}$	Forward	48,156	22,832
	Reverse	25,324	
$\text{CO}_2^{**} \rightleftharpoons \text{CO}^* + \text{O}^*$	Forward	794	787
	Reverse	7	
$\text{CO}_2^{**} + \text{H}\# \rightleftharpoons \text{HCOO}^{**}$	Forward	232,138	22,045
	Reverse	210,093	
$\text{H}_2\text{COOH}^{**} \rightleftharpoons \text{H}_2\text{CO}^* + \text{OH}^*$	Forward	30,531,530	18,635
	Reverse	30,512,895	
$\text{CO}^* + \text{H}\# \rightleftharpoons \text{HCO}^*$	Forward	12,989	−4851
	Reverse	17,840	
$\text{H}_2\text{CO}^* + \text{H}\# \rightleftharpoons \text{H}_3\text{CO}^*$	Forward	30,196	13,784
	Reverse	16,412	
$\text{CO}^* \rightleftharpoons \text{CO} + ^*$	Forward	28,343,079	5638
	Reverse	28,337,441	
$\text{H}_3\text{COH}^* \rightleftharpoons \text{H}_3\text{COH} + ^*$	Forward	120,976	10,779
	Reverse	110,197	

^a * and ** represent the monodentate and the bidentate species, respectively.

^b # represents the adsorption site on Cu.

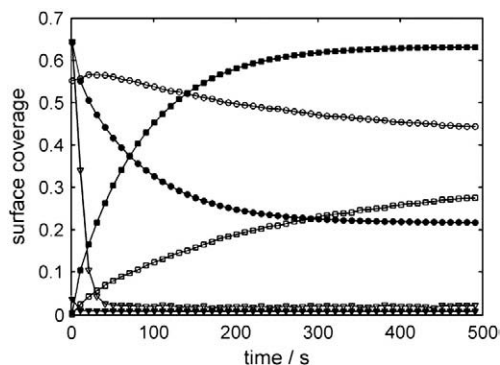


Fig. 6. Comparison between microkinetics and kMC results for the coverage of surface species. Solid curves: microkinetics results; Open curves: kMC results. Square: H_3CO^* ; Circle: HCOO^* ; Triangle: empty site ($\times 5$).

bidentate species and needs two empty sites for adsorption. In kMC, the algorithm counts the number of two neighboring empty sites and calculates the probability for CO₂ adsorption. By contrast, the rate is simply calculated as kc_{empty}^2 in microkinetics, which means that single empty site will also contribute to the adsorption rate of CO₂. Therefore, the adsorption rate is always larger in microkinetics, which results in a lower concentration of empty sites.

Similarly, the higher coverage of H₃CO and the lower coverage of HCOO from microkinetic simulation (as shown in Fig. 6) are caused by the mean-field approximation. For the elementary step $\text{H}_2\text{COOH}^{**} = \text{H}_2\text{CO}^* + \text{OH}^*$, we noticed that the rates of the reverse reaction differ greatly between these two methods. While kMC counts the number of neighboring OH and H₂CO pair, the rate is calculated as $kc_{\text{H}_2\text{COCOH}}$ in microkinetics. Once H₂CO and OH are produced, most of them will couple back into H₂COOH instead of diffusing along the interface, because H₂COOH is much more stable and the barrier for the reverse reaction is quite low. The rate expression in microkinetics underestimates the rate of reverse reaction with the assumption that reactants have been mixed completely before they react with each other. As a result, there are more H₃CO on the surface in microkinetic simulation.

It should be emphasized that the mean-field approximation in microkinetics may not be a valid assumption for heterogeneous catalytic reactions in general. The assumption may work well for the reaction in the gas phase or in solution because the mixing of reactants is usually much faster than the reaction itself. However, on the surface of catalysts the diffusion is often kinetically hindered (e.g. a corrugated potential energy surface or local high surface coverage), which does not guarantee that the rate expression in microkinetics is correct. For CO₂ hydrogenation on Cu/ZrO₂ interface, we noticed that the adsorbed CO₂, HCOO and H₂COO are hard to diffuse since they are bidentate species with high adsorption energies on the oxide Zr sites. The diffusion on the oxide sites is intrinsically difficult also because of the large lattice separation between Zr ions.

4.2. Importance of secondary reactions due to the readsorption of products

As shown in Table 3, before a methanol molecule flows out of the reaction chamber, it may adsorb and desorb on the catalyst for more than 10 times. This value for CO is about 5000. Since the contact time in reality is usually several seconds, the product molecules can well have the chance to hit to the catalyst, which can lead to the secondary reaction process. It is therefore essential to take into account the readsorption of products to simulate the reaction at the experimental conditions.

To demonstrate the importance of the secondary reactions, we carried out a kMC simulation by neglecting completely the readsorption processes of CO, H₃COH and H₂O. The simulation without the readsorption process increases the formation rates of CO and H₃COH by a factor of 3 and 1.5, respectively. The selectivity to methanol is reduced to 52%. In addition, the surface composition is significantly different. The coverage of H₃CO is only 1/6 of that in the full simulation and the coverages of OH and O decrease by about 1000 times. As a result, there are much more empty sites on the surface, about 20 times more than that in the full simulation. Based on these, we can conclude that the secondary reactions are important at the experimental conditions, which lower the overall TOF but increase the selectivity towards methanol.

5. Conclusion

This work represents our theoretical attempt to compare fully the DFT-based kinetic Monte Carlo simulation results with the experimental data for CO₂ fixation on Cu/ZrO₂ surface. The free energy profiles for the reaction are established from DFT with all ZPE

correction and entropy effect included. Two types of kinetics simulation are carried out, namely, the equilibrium simulation in a closed system and the dynamic simulation based on the continuous stirred tank reactor model.

Our equilibrium simulation shows that CO₂ conversions to H₃COH and CO are 12.5% and 6.2% respectively, in a good agreement with the values derived from experimental thermodynamics data. From the dynamic simulation, the following results are obtained. (i) Most (>90%) of CO₂ molecules are hydrogenated to formate, while only few of them decompose to CO. Both methanol and CO are produced dominantly via the formate pathway. We found that the dissociation of CO₂ is the slowest step. H₂CO is a key intermediate species in the reaction pathway, the hydrogenation of which dictates the high temperature of CO₂ hydrogenation. (ii) Formate, H₂COO and CO are formed instantaneously as the reaction starts and their concentrations hardly change during the reaction. On the contrary, H₃CO is low in concentration at the beginning, but its coverage continuously increases at the first ten minutes of the reaction. (iii) The conversion of CO₂ is 1.2% with the selectivity to H₃COH being 68%. The TOF is calculated to be $2.4 \times 10^{-3} \text{ s}^{-1}$. These values are in the range of experimental measurement. (iv) The calculated apparent activation energy for CO and methanol formation are 1.79 and 0.79 eV, respectively. This explains why the selectivity to methanol decreases dramatically as the temperature increases. (v) the secondary reactions due to the readsorption of products lower the overall TOF but increase the selectivity to methanol by 16%. (vi) By comparing the kMC simulation results with the microkinetics results, we found that the mean-field assumption in microkinetics is not valid for the reaction at the metal/oxide interface. The overall rate from microkinetic simulation is overestimated.

Acknowledgements

This work is supported by NSF of China (20825311, 20773026, 20721063), Sci. & Tech. Comm. of Shanghai Municipality (08DZ2270500) and Program for Professor of Special Appointment (Eastern Scholar) at Shanghai Institute of Higher Learning.

References

- [1] D. R. Lide, CRC Handbook of Chemistry and Physics, 89th ed., CRC Press, Boca Raton, 2009, Sect5, pp. 13, pp. 20, pp. 46, pp. 49, pp. 57.
- [2] J. Yoshihara, S. Parker, A. Schafer, C.T. Campbell, Catal. Lett. 31 (1995) 313.
- [3] J. Yoshihara, C.T. Campbell, J. Catal. 161 (1996) 776.
- [4] A. Baiker, D. Gasser, Appl. Catal. 48 (1989) 279.
- [5] R.A. Koepfel, A. Baiker, C. Schild, A. Wokaun, Stud. Surf. Sci. Catal. 63 (1991) 59.
- [6] E. Shustorovich, A.T. Bell, Surf. Sci. 253 (1991) 386.
- [7] N. Kanoun, M.P. Astier, G.M. Pajonk, Catal. Lett. 15 (1992) 231.
- [8] R.A. Koepfel, A. Baiker, A. Wokaun, Appl. Catal. A 84 (1992) 77.
- [9] Y. Sun, P.A. Sermon, J. Chem. Soc. Chem. Commun. 16 (1993) 1242.
- [10] Y. Nitta, O. Suwata, Y. Ikeda, Y. Okamoto, T. Imanaka, Catal. Lett. 26 (1994) 345.
- [11] Y. Sun, P.A. Sermon, Catal. Lett. 29 (1994) 361.
- [12] I.A. Fisher, H.C. Woo, A.T. Bell, Catal. Lett. 44 (1997) 11.
- [13] I.A. Fisher, A.T. Bell, J. Catal. 172 (1997) 222.
- [14] K.-D. Jung, A.T. Bell, J. Catal. 193 (2000) 207.
- [15] J. Weigel, R.A. Koepfel, A. Baiker, A. Wokaun, Langmuir 12 (1996) 5319.
- [16] J. Wambach, A. Baiker, A. Wokaun, Phys. Chem. Chem. Phys. 1 (1999) 5071.
- [17] A.A. Gokhale, J.A. Dumesic, M. Mavrikakis, J. Am. Chem. Soc. 130 (2008) 1402.
- [18] Q.-L. Tang, Q.-J. Hong, Z.-P. Liu, J. Catal. 263 (2009) 114.
- [19] J.M. Soler, E. Artacho, J.D. Gale, A. Garcia, J. Junquera, P. Ordejon, D. Sanchez-Portal, J. Phys. Condens. Matter 14 (2002) 2745.
- [20] J. Junquera, O. Paz, D. Sanchez-Portal, E. Artacho, Phys. Rev. B 64 (2001) 235111.
- [21] J.P. Perdew, K. Burke, M. Ernzerhof, Phys. Rev. Lett. 77 (1996) 3865.
- [22] N. Troullier, J.L. Martins, Phys. Rev. B 43 (1991) 1993.
- [23] E. Artacho, D. Sanchez-Portal, P. Ordejon, A. Garcia, J.M. Soler, Phys. Status Solidi B 215 (1999) 809.
- [24] H.-F. Wang, Z.-P. Liu, J. Am. Chem. Soc. 130 (2008) 10996.
- [25] G. Henkelman, H. Jonsson, J. Chem. Phys. 111 (1999) 7010.
- [26] C. Shang, Z.-P. Liu, J. Chem. Theory Comput. 6 (2010) 1136.
- [27] K.T. Jung, A.T. Bell, Catal. Lett. 80 (2002) 63.
- [28] A. Christensen, E.A. Carter, Phys. Rev. B 58 (1998) 8050.
- [29] B. Bachiller-Baeza, I. Rodriguez-Ramos, A. Guerrero-Ruiz, Langmuir 14 (1998) 3556.
- [30] A. Chatterjee, D.G. Vlachos, J. Comput.-Aided Mater. Des. 14 (2007) 253.

- [31] G. Gilmer, *Science* 208 (1980) 355.
- [32] K. Reuter, D. Frenkel, M. Scheffler, *Phys. Rev. Lett.* 93 (2004) 116105.
- [33] M. Neurock, S.A. Wasileski, D. Mei, *Chem. Eng. Sci.* 59 (2004) 4703.
- [34] C. Sendner, S. Sakong, A. Cross, *Surf. Sci.* 600 (2006) 3258.
- [35] A. La Magna, S. Coffa, L. Colomo, *Phys. Rev. Lett.* 82 (1999) 1720.
- [36] A.C. Levi, M. Kotrla, *J. Phys. Condens. Matter* 9 (1997) 299.
- [37] X. Ren, P. Rinke, M. Scheffler, *Phys. Rev. B* 80 (2009) 045402.
- [38] K.A. Koepfel, A. Baiker, A. Wokaun, *Appl. Catal. A* 84 (1992) 77.
- [39] R. Ziff, E. Gulari, Y. Barshad, *Phys. Rev. Lett.* 56 (1986) 2553.
- [40] J.W. Evans, D.J. Liu, M. Tammaro, *Chaos* 12 (2002) 131.
- [41] V.P. Zhdanov, *Surf. Sci.* 500 (2002) 966.
- [42] E. Clement, P. Leroux-Hugon, L. Sander, P. Argyrakos, *J. Phys. Chem.* 98 (1994) 7274.
- [43] B. Temel, H. Meskine, K. Reuter, M. Scheffler, H. Metiu, *J. Chem. Phys.* 126 (2007) 204711.
- [44] A.K. Jain, R.R. Hudgins, P.L. Silveston, *Can. J. Chem. Eng.* 61 (1983) 46.